nature communications

Article

https://doi.org/10.1038/s41467-025-67880-5

Possible liquid-nitrogen-temperature superconductivity driven by perpendicular electric field in the single-bilayer film of $La_3Ni_2O_7$ at ambient pressure

Received: 9 May 2025

Accepted: 10 December 2025

Published online: 03 January 2026

Check for updates

Zhi-Yan Shao[1,7], Jia-Heng Ji[1,7], Congjun Wu[2,3,4,5], Dao-Xin Yao[6] & Fan Yang[1]

Recently, high-temperature superconductivity (HTSC) is found in the $La_3Ni_2O_7/SrLaAlO_4$ ultrathin film with critical temperature T_c above the McMillan limit at ambient pressure (AP). It is eager to enhance T_c of $La_3Ni_2O_7$ at AP. We propose that a perpendicular electric field strongly enhances T_c in the single-bilayer film of $La_3Ni_2O_7$ at AP. Under electric field, the layer with lower potential energy will accept electrons flowing from the other layer to fill in the Ni-$3d_{x^2-y^2}$ orbitals, as the nearly half-filled Ni-$3d_{z^2}$ orbital cannot accommodate more electrons. With the enhancement of the filling fraction in the $3d_{x^2-y^2}$ orbitals in this layer, the interlayer *s*-wave pairing is suppressed, but the intralayer *d*-wave pairing in this layer is strongly enhanced. We numerically verify this idea and yield that an imposed voltage of about 0.1 ~ 0.2 volt between layers is enough to realize liquid-nitrogen-temperature HTSC in this single bilayer at AP. Our results appeal for experimental verification.

The discovery of superconductivity (SC) with critical temperature T_c above the boiling point of liquid nitrogen (≈ 77 K) in the pressurized $La_3Ni_2O_7$[1–9] has attracted great interests[10–144]. This discovery has sparked the exploration of high-temperature SC (HTSC) in Ruddlesden-Popper phase multilayer nickelates, resulting in the discovery of SC in the pressurized $La_4Ni_3O_{10}$[39–45], which together with the previously synthesized infinite-layer nickelates $Nd_{1-x}Sr_xNiO_2$[46–49] have established a new family of SC other than cuprates and iron-based superconductors. However, the high pressure (HP) circumstance not only strongly hinders the experimental detection of the samples but also brings difficulties in the application of SC in industry. Very recently, the $La_3Ni_2O_7$ ultrathin film with a few layers of unit cell grown on the $SrLaAlO_4$ (SLAO) substrate has been grown by two different groups independently and SC with T_c above the McMillan limit (≈ 40 K) has been detected at ambient pressure (AP)[132–134], allowing various experimental investigation of the pairing mechanism in this material, attracting a lot of interests[135–144]. It is now eager to enhance the T_c of this material at AP. Here we propose a viable approach to realize T_c above the boiling point of liquid nitrogen in the $La_3Ni_2O_7$ single-bilayer film at AP.

Presently, the pairing mechanism in the $La_3Ni_2O_7$, either in the bulk material under HP[74–100,104–108,125–128] or in the ultrathin film at AP[135,138,140,143], is still under debate. Density-functional-theory (DFT) based first-principle calculations have suggested that the low-energy orbitals are mainly Ni-$3d_{z^2}$ and $3d_{x^2-y^2}$, which are nearly half- and quarter- filled[50–58,61]. Various experiments have revealed the strongly-correlated characteristic of the material[14,16,22,24,25,28,31,32]. Particularly, the

[1]School of Physics, Beijing Institute of Technology, Beijing, China. [2]New Cornerstone Science Laboratory, Department of Physics, School of Science, Westlake University, Hangzhou, Zhejiang, China. [3]Institute for Theoretical Sciences, Westlake University, Hangzhou, Zhejiang, China. [4]Key Laboratory for Quantum Materials of Zhejiang Province, School of Science, Westlake University, Hangzhou, Zhejiang, China. [5]Institute of Natural Sciences, Westlake Institute for Advanced Study, Hangzhou, Zhejiang, China. [6]Guangdong Provincial Key Laboratory of Magnetoelectric Physics and Devices, State Key Laboratory of Optoelectronic Materials and Technologies, Center for Neutron Science and Technology, School of Physics, Sun Yat-Sen University, Guangzhou, China. [7]These authors contributed equally: Zhi-Yan Shao, Jia-Heng Ji. e-mail: yangfan_blg@bit.edu.cn

optical study reveals significant reduction of the electron kinetic energy which places the system in the proximity of the Mott phase[25]; the angle-resolved photoemission spectroscopy uncovers strong band renormalization caused by electron correlation[28]; the linearly temperature-dependent resistivity suggests "strange-metal" behavior[2]. Therefore, we take a strong-coupling view of the system. Under the strong Hubbard repulsion, the nearly half-filled $3d_{z^2}$ electrons can almost be viewed as localized spins. Therefore, the main carrier of SC should be the $3d_{x^2-y^2}$ electrons, which subject to the in-plane superexchange interaction just mimic the 50% hole-doped cuprates. However, it is a problem how HTSC can emerge under such a high doping level. The key physics lies in the important role played by the $3d_{z^2}$ orbitals. Through strong interlayer perpendicular superexchange, the $3d_{z^2}$ electrons form interlayer pairing. The interlayer perpendicular superexchange or the interlayer pairing of the $3d_{z^2}$ electrons can be transmitted to the $3d_{x^2-y^2}$ electrons through the Hund's rule[79,80,82,87,92,93,95–98,100,107,108] or the nearest-neighbor (NN) hybridization[65,83,86,87,91,98,105,107,108] or both. Under such view, the role of pressure in enhancing the T_c lies in the enhancement of the interlayer perpendicular superexchange, the inter-orbital hybridization, or both.

In this work, we propose an alternative approach to realize HTSC with T_c above the boiling point of liquid nitrogen in the ultrathin film of $La_3Ni_2O_7$ at AP. Here we consider the thinnest limit, i.e. a single bilayer film of $La_3Ni_2O_7$, and realize the goal by introducing charge transfer with a perpendicular electric field, which let the electrons flow from the high-energy layer to the low-energy layer, similar to the mechanism for the spontaneous charge transfer in oxide heterostructures[145–150]. The external electric field based approach avoids introducing disorder as in chemical doping[151] or exhibiting orbital selectivity based on symmetry[152], demonstrating exceptional performance in the field of twisted multilayer graphene materials[153–155]. We can impose a perpendicular electric field, say pointing upward, in this single bilayer, so that electrons from the top layer will flow to the bottom layer. These electrons will fill the $3d_{x^2-y^2}$ orbitals in the bottom layer as the nearly half-filled $3d_{z^2}$ orbitals there cannot accommodate more electrons. The enhancement of the bottom-layer $3d_{x^2-y^2}$ electron number will first suppress the interlayer *s*-wave SC due to mismatch of the electron numbers between the two layers, similar with the case in which an imposed Zeeman field acting on the spin leads to mismatch of the electron numbers between the two spin species and thus suppresses singlet pairing, and then promptly lead to the intra-bottom-layer *d*-wave SC with strongly enhanced T_c. To test this idea, we have performed a combined simplified single orbital study and a comprehensive two orbital study, which consistently yield that a voltage of experimentally achievable levels (around 0.1 ~ 0.2 volt predicted by the mean-field calculations) between the two layers is enough to induce *d*-wave SC with T_c above the boiling point of liquid nitrogen in the bottom layer. Intriguingly, the *d*-wave SC carried by the bottom layer $3d_{x^2-y^2}$ electrons coexists with the interlayer *s*-wave pseudo gap carried by the $3d_{z^2}$ electrons in the mixing ratio of 1: i, breaking time-reversal symmetry. Our proposal potentially provides a viable approach to realize HTSC with T_c above the boiling point of liquid nitrogen in the single bilayer film of $La_3Ni_2O_7$.

Results

Consideration and a simplified study

The $La_3Ni_2O_7$ ultrathin film grown on the SLAO substrate form a bilayer square lattice[135,137]. As illustrated in Fig. 1a, the leading hopping integrals are the interlayer hopping of the $3d_{z^2}$ electrons $t_\perp$ and the intralayer NN hopping of the $3d_{x^2-y^2}$ electrons $t_\parallel$. Under strong Hubbard U, these hopping terms can induce the effective superexchange $J_\perp$ and $J_\parallel$ through $J \approx \frac{4t^2}{U}$. Under the Hund's rule coupling J_H, the spins of the two orbitals are inclined to be parallel aligned, as illustrated in Fig. 1b, which partly transmits the interlayer perpendicular superexchange $J_\perp$ between the $3d_{z^2}$ orbitals to the $3d_{x^2-y^2}$ orbitals as $\tilde{J}_\perp = \alpha J_\perp$ with $\alpha \in (0, 1)$ describing the efficiency of this process and related to the strength of Hund's coupling J_H. In addition, there exists intralayer NN- hybridization t_{xz} between the two orbitals. As shown in Fig. 2(a, b), the nearly quarter-filled $3d_{x^2-y^2}$ electrons subject to $J_\parallel$ and $\tilde{J}_\perp$ form interlayer-dominant pairing[79].

Now let us turn on the upward electric field $\boldsymbol{\varepsilon}$, forcing electrons downward, as shown in Fig. 2(c, d). In the top layer, since the $3d_{z^2}$ orbitals host larger density of state (DOS) than the $3d_{x^2-y^2}$ orbitals, they will donate more electrons. Most of these donated electrons will fill the $3d_{x^2-y^2}$ orbitals in the bottom layer, as the nearly half-filled $3d_{z^2}$ orbitals there cannot accommodate more electrons. A minority of the donated electrons can also be accepted by the top-layer $3d_{x^2-y^2}$ orbitals.

Even with doped holes under $\boldsymbol{\varepsilon}$, the top-layer $3d_{z^2}$ electrons cannot carry SC: Firstly, lacking pairing interaction, they cannot form intralayer pairing. Secondly, although they can pair with the localized bottom-layer $3d_{z^2}$ electrons, such pairs cannot coherently move, only resulting in the pseudo-gap. Therefore, the SC under $\boldsymbol{\varepsilon}$ can only be carried by the $3d_{x^2-y^2}$ orbitals. As the filling fractions of the $3d_{x^2-y^2}$ orbitals in the two layers are different, their Fermi levels are relatively shift, leading to mismatch of their Fermi surfaces (FSs), which will suppress their interlayer pairing. Here the perpendicular electric field acts as a "pseudo-Zeeman field" acting on the layer index, just like the Zeeman field acting on the spin degree of freedom. The bottom-layer $3d_{x^2-y^2}$ orbitals will form *d*-wave SC, mimicsing the cuprates, as shown in Fig. 2(d). When $\boldsymbol{\varepsilon}$ is strong enough so that the filling fraction of the bottom-layer $3d_{x^2-y^2}$

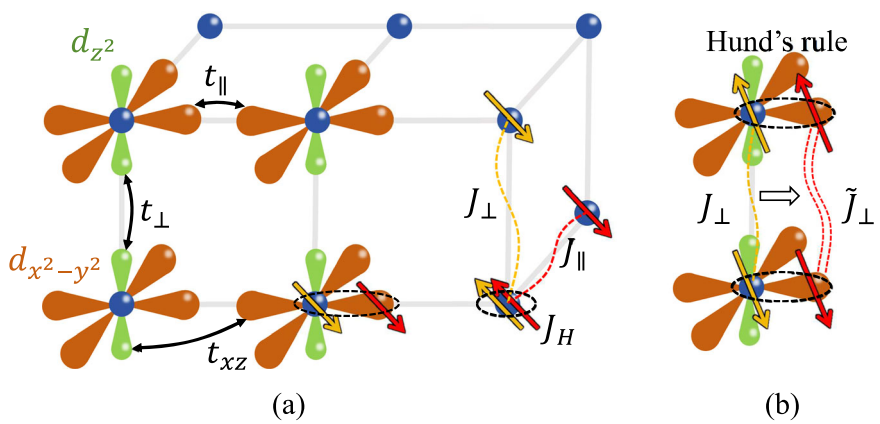

Fig. 1 | Schematic diagrams of the model. a Schematic diagram for the dominant hopping integrals and superexchange interactions between the E_g orbitals in $La_3Ni_2O_7$. **b** Schematic diagram illustrating that the Hund's rule coupling transmits the interlayer perpendicular superexchange interaction $J_\perp$ between the $3d_{z^2}$ orbitals to the effective one $\tilde{J}_\perp$ between the $3d_{x^2-y^2}$ orbitals.

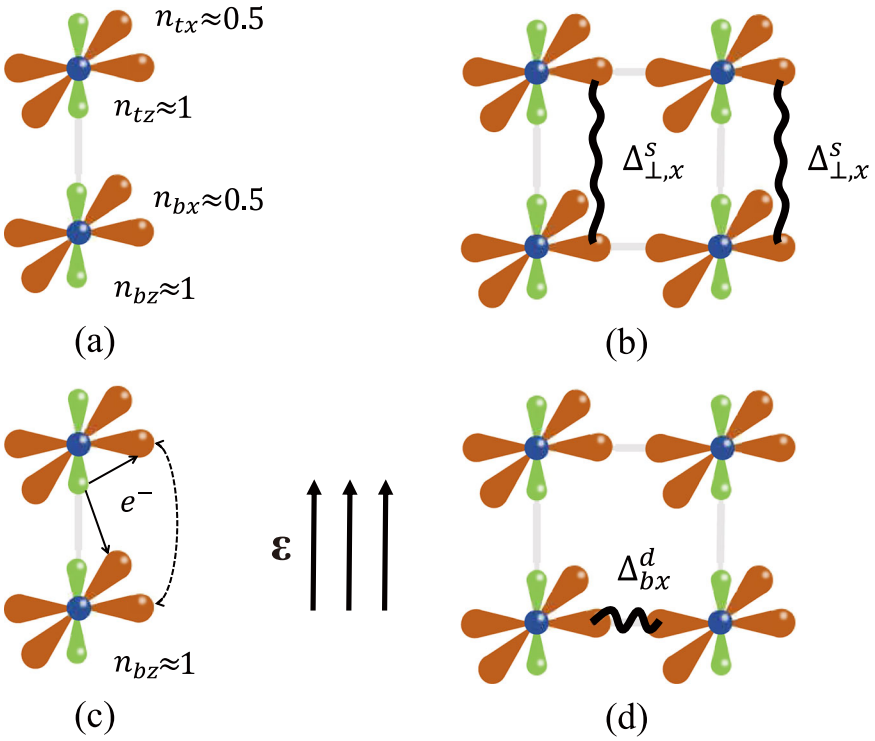

Fig. 2 | Schematic diagrams of particle number and pairing configuration before and after introducing perpendicular electric field. a Particle numbers of the four E_g orbitals within an unit cell without electric field. **b** The dominant pairing configuration for (**a**). **c** Schematic diagram showing how the electrons flow under the perpendicular electric field $\boldsymbol{\varepsilon}$ pointing upward. **d** The dominant pairing configuration for (**c**).

orbitals is near that of the optimal doped cuprates, *d*-wave HTSC with strongly enhanced T_c will be achieved in this layer, and the top layer will also acquire SC below T_c through proximity.

Based on the above general consideration, we first conduct the following simplified model study including only the $3d_{x^2-y^2}$-orbital, with the $3d_{z^2}$ orbital only viewed as a source which tunes the total electron number. The following widely adopted single $3d_{x^2-y^2}$-orbital bilayer $t-J-J_\perp$ model[79,80,82,92,93,95,96,100] is adopted,

$$\begin{aligned} H &= -t_\parallel \sum_{\langle i,j\rangle,\mu,\sigma} \widehat{P}\left(c^\dagger_{i\mu\sigma}c_{j\mu\sigma}+\text{h.c.}\right)\widehat{P}+\sum_{i,\mu}\epsilon_\mu n_{i\mu} \\ &\quad +J_\parallel \sum_{\langle i,j\rangle,\mu}\mathbf{S}_{i\mu}\cdot\mathbf{S}_{j\mu}+\widetilde{J}_\perp\sum_i \mathbf{S}_{it}\cdot\mathbf{S}_{ib}. \end{aligned} \tag{1}$$

Here $c^\dagger_{i\mu\sigma}$ creates an electron at site i in the layer μ (=top (t)/bottom (b)) with spin σ, $\widehat{P}$ is a projection operator projecting out the double occupancy of all site, and $n_{i\mu}$ or $\mathbf{S}_{i\mu}$ denote the corresponding electron number or spin operator. Only NN- bond $\langle i,j\rangle$ is considered in the summation. The ϵ_μ is introduced to control the filling fractions of the two layers under $\boldsymbol{\varepsilon}$, with $\epsilon_t-\epsilon_b=\varepsilon$. However, as the total particle number of the $d_{x^2-y^2}$ electrons under given $\boldsymbol{\varepsilon}$ is unknown, we have to assume the ratio r: 1 between the electron number flowing from the $3d_{z^2}$ orbitals and that flowing from $3d_{x^2-y^2}$ orbitals in the top layer when solving the model with the standard slave-boson mean-field (SBMF) theory[156], which demonstrates exceptional performance for $La_3Ni_2O_7$ in previous studies[79,80] that is qualitatively consistent with experimental data[1] and theoretical studies using other numerical methods (like DMRG)[82,92,96]. Due to reason of DOS, we assume this ratio to be 2: 1, with details provided in the Supplementary Information (SI). Nevertheless, the concrete value of this ratio turns out not to obviously affect the results (see the SI). The filling fractions are fixed under this assumption in the SBMF study. To capture the quantum fluctuation beyond mean-field, the density matrix renormalization group (DMRG)[157,158] method is also employed, whose results are qualitatively consistent with those of the SBMF study, indicating that the SBMF theory can capture the main features of this system. See details in the *Methods* and SI.

We set $t_\parallel=1$ as the energy unit and $J_\parallel=0.4t_\parallel$ in our study. $\widetilde{J}_\perp=(1-\delta_{tz})\times1.3J_\parallel$ is applied in our SBMF study. The results are shown in Fig. 3. Figure 3(a) shows the amplitude and symmetry of the ground-state pairing gap as function of the bottom-layer $3d_{x^2-y^2}$ electron number n_{bx}, whose value enhances with $\boldsymbol{\varepsilon}$. It is shown that when $\boldsymbol{\varepsilon}$ or n_{bx} enhances, the pairing amplitude $\widetilde{\Delta}$ decays first and then increases. When $n_{bx}=0.5$, the ground state is confirmed to be interlayer *s*-wave SC by comparing the energies of states with different symmetries (See SI for more details). Then the *s*-wave pairing is suppressed by the enhancement of ε or n_{bx} because of the mismatch of the FSs of the two layers caused by ε, similar to the case of a singlet pairing state placed within a pair-breaking Zeeman field. Therefore, it is also possible that this "pseudo Zeeman field" can drive pair density wave (PDW), just like that the real Zeeman field can drive the Fulde-Ferrell-Larkin-Ovchinnikov state. When $n_{bx}\geq0.53$, the ground state is an intralayer *d*-wave SC, with the dominant pairing limited in the bottom layer. It is inspiring that with the enhancement of n_{bx} in this regime, the $\widetilde{\Delta}$ enhances promptly, similar to the case in the overdoped cuprates, wherein the enhancement of the filling fraction promptly enhances the pairing strength. The pairing configurations of the two different pairing symmetries are illustrated in Fig. 3(c, d).

The T_c ~ n_{bx} is shown in Fig. 3(b). In the SBMF theory, the T_c is given as the lower one between the spinon-pairing temperature T_{pair} and the holon-BEC temperature T_{BEC}. The inset of Fig. 3(b) displays $T_{\text{BEC}}\gg T_{\text{pair}}$, rendering $T_c=T_{\text{pair}}$ in the considered n_{bx} regime. Note that the T_c here is in the sense of Kosterlitz-Thouless transition. A comparison between Fig. 3(b) and (a) suggests that T_c scales with $\widetilde{\Delta}$, which is more clear when the T_c ~ n_{bx} is well fitted by $0.42\widetilde{\Delta}\sim n_{bx}$ for the *d*-wave and $0.9\widetilde{\Delta}\sim n_{bx}$ for the *s*-wave in Fig. 3(b), consistent with the Bardeen-Cooper-Schrieffer (BCS) theory. Inspiringly, for $n_{bx}\geq0.75$, the $T_c\gtrsim0.02t_\parallel\approx80$ K, suggesting the HTSC in the liquid nitrogen temperature range.

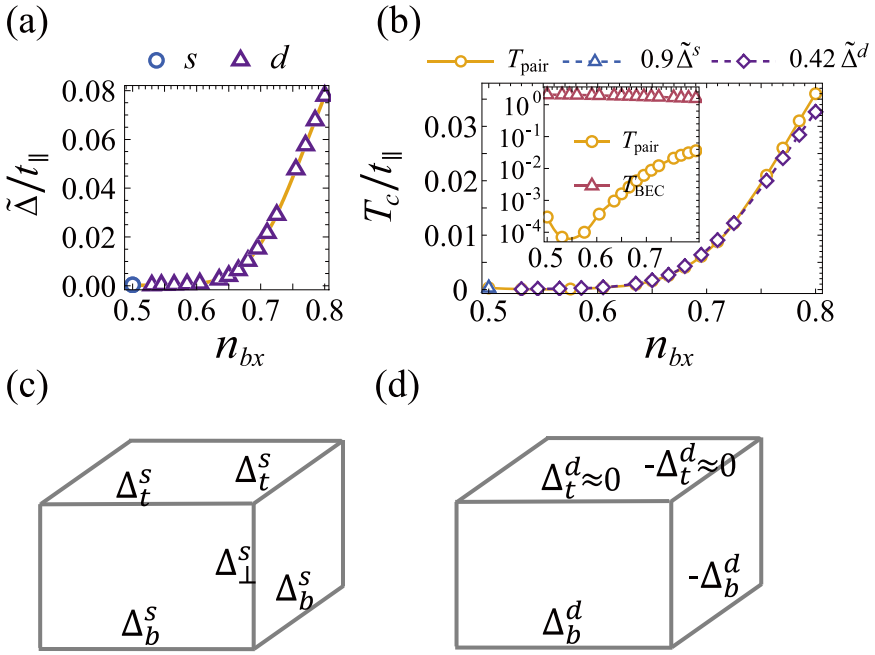

Fig. 3 | The SBMF results for the single-orbital model. a The pairing amplitude $\tilde{\Delta}$ (in unit of $t_{\parallel}$) as function of the bottom-layer particle number per site n_{bx}. Different pairing symmetries are distinguished by color. **b** The T_c as function of n_{bx}, in comparison with $0.42\tilde{\Delta}$ for the *d*-wave and $0.9\tilde{\Delta}$ for the *s*-wave regime. Inset: the spinon pairing temperature $T_{\rm pair}$ and the holon condensation temperature $T_{\rm BEC}$ as function of n_{bx}. In (**a**, **b**), we set $J_{\parallel} = 0.4t_{\parallel}$ and $\tilde{J}_{\perp} = (1-\delta_{tz}) \times 1.3J_{\parallel}$. **c**, **d** The pairing configurations of the *s*-wave and *d*-wave, respectively.

On the above, we have adopted $\tilde{J}_{\perp} = \alpha J_{\perp}(1-\delta_{tz})$ with $\alpha = 1$, where δ_{tz} denotes the hole density of the top-$3d_{z^2}$ orbital. For the reduced α, only the low-n_{bx} regime accommodating the interlayer *s*-wave pairing in Fig. 3(a, b) shrinks but the high-n_{bx} regime accommodating the intralayer *d*-wave SC is not affected because the intralayer pairing is blind to $\tilde{J}_{\perp}$. Furthermore, assuming different ratios between the changes of the filling fractions of the two top-layer E_g orbitals turns out to yield similar results when expressed as functions of n_{bx}, as the dominant pairing under strong $\boldsymbol{\varepsilon}$ is the intra-bottom-layer pairing, which is blind to the filling fraction of the top layer. See the SI for details.

We have further employed the DMRG approach, which can capture the quantum fluctuation beyond mean-field, to compute the ground state of Hamiltonian (1) under different electric fields ε and the transferred electron-doping levels of the $d_{x^2-y^2}$ orbitals $\delta = n_{tx} + n_{bx} - 1$. For $\varepsilon = 0$, we have $\delta = 0$. When ε increases, it drives electrons from d_{z^2}-orbitals in the top layer to $d_{x^2-y^2}$-orbitals in both layers, increasing δ. However, as the exact relationship between ε and δ is unclear, we set them as two independent variables in our DMRG study. The parameters $t_{\parallel}$ and $J_{\parallel}$ take the same values as the ones in the SBMF study while $\tilde{J}_{\perp} = 0.8J_{\parallel}$ is adopted in the DMRG study. To characterize the pairing symmetry and strength, we analyze the interlayer pairing correlation function $\Phi^{\perp}(r)$ and the intra-bottom-layer pairing correlation function $\Phi_b^{\parallel}(r)$. More details are provided in *Methods*.

Figure 4 (a) shows the pairing phase diagram with respect to δ ($= 0, 1/16, 1/8$) and ε ($\in [0, 1.6t_{\parallel}]$). Figure 4(b) shows the absolute value of the intra-bottom-layer pairing correlation functions $|\Phi_b^{\parallel}(r)|$ under different electric fields $\varepsilon = 0$, $0.4t_{\parallel}$, $0.8t_{\parallel}$, $1.2t_{\parallel}$, $1.6t_{\parallel}$ for $\delta = 0$, and the results for $\delta = 1/16$ are presented in Fig. 4(c). It turns out that $|\Phi_b^{\parallel}(r)|$ exhibits algebraic decay under an non-zero external electric field with the decaying power exponent to be $K_{\rm SC}$, i.e. $|\Phi_b^{\parallel}(r)| \propto r^{-K_{\rm SC}}$ for large enough r, implying the presence of pairing within the bottom layers. Figure 4(d) and (e) depict $|\Phi_b^{\parallel}(r)|$ for different transferred $d_{x^2-y^2}$-electron-doping levels $\delta = 0, 1/16, 1/8$ under $\varepsilon = 0.4t_{\parallel}$ in (d) and $\varepsilon = 0.8t_{\parallel}$ in (e). All the algebraic decay exponents $K_{\rm SC}$ are provided accordingly.

The results indicate that (i) With the enhancement of the perpendicular electric field ε, and hence the transferred $d_{x^2-y^2}$-electron-doping level δ, the pairing symmetry changes from interlayer *s*-wave to intra-bottom-layer *d*-wave (The criterion of the pairing symmetry is provided in *Methods*); (ii) For all the transferred $d_{x^2-y^2}$-electron-doping levels δ tested, the enhancement of the perpendicular electric field ε leads to a reduction of $K_{\rm SC}$, suggesting the enhancement of the intra-bottom-layer pairing; (iii) Under all the perpendicular electric field strengths ε tested, the enhancement of the transferred $d_{x^2-y^2}$-electron-doping level δ leads to a reduction of $K_{\rm SC}$, suggesting the enhancement of the intra-bottom-layer pairing. From (ii) and (iii), it is clear that the enhancement of ε and hence δ will significantly enhance the intra-bottom-layer pairing. These results are qualitatively consistent with those of the SBMF study. More results are given in the SI.

Besides, we study the effect of interlayer Coulomb interaction. Our results show that the interlayer Coulomb interaction slightly promotes charge transfer between layers and the intra-bottom-layer pairing, while suppressing the interlayer pairing. See SI for details.

The comprehensive two-orbital study

The above simplified single-orbital study has drawbacks: We cannot determine the relationship between the electron-doping of the $d_{x^2-y^2}$ orbitals and the electric field. In the SBMF study, we have to assume the ratio between the changes of the filling fractions of the two top-layer E_g orbitals. In addition, we do not know how the neglected $3d_{z^2}$ orbital degree of freedom affects the pairing nature. To settle these puzzles, we conduct a comprehensive two-orbital model[107] to study with,

$$
\begin{aligned}
H = & -t_{\parallel} \sum_{\langle i,j\rangle,\mu} \hat{P}\left(c_{i\mu x\sigma}^{\dagger} c_{j\mu x\sigma} + \text{h.c.}\right)\hat{P} - t_{\perp} \sum_{i} \hat{P}\left(c_{itz\sigma}^{\dagger} c_{ibz\sigma} + \text{h.c.}\right)\hat{P} \\
& - t_{xz} \sum_{\langle i,j\rangle\mu} \hat{P}\left(c_{i\mu x\sigma}^{\dagger} c_{j\mu z\sigma} + (z \leftrightarrow x) + \text{h.c.}\right)\hat{P} + J_{\parallel} \sum_{\langle i,j\rangle\mu} \mathbf{S}_{i\mu x} \cdot \mathbf{S}_{j\mu x} \\
& + J_{\perp} \sum_{i} \mathbf{S}_{itz} \cdot \mathbf{S}_{ibz} + \tilde{J}_{\perp} \sum_{i} \mathbf{S}_{itx} \cdot \mathbf{S}_{ibx} + \epsilon_z \sum_{i\mu\sigma} n_{i\mu z\sigma} + \epsilon_x \sum_{i\mu\sigma} n_{i\mu x\sigma} \\
& + \frac{\varepsilon}{2} \sum_{ia\sigma} n_{ita\sigma} - \frac{\varepsilon}{2} \sum_{ia\sigma} n_{iba\sigma}.
\end{aligned}
\tag{2}
$$

https://doi.org/10.1038/s41467-025-67880-5

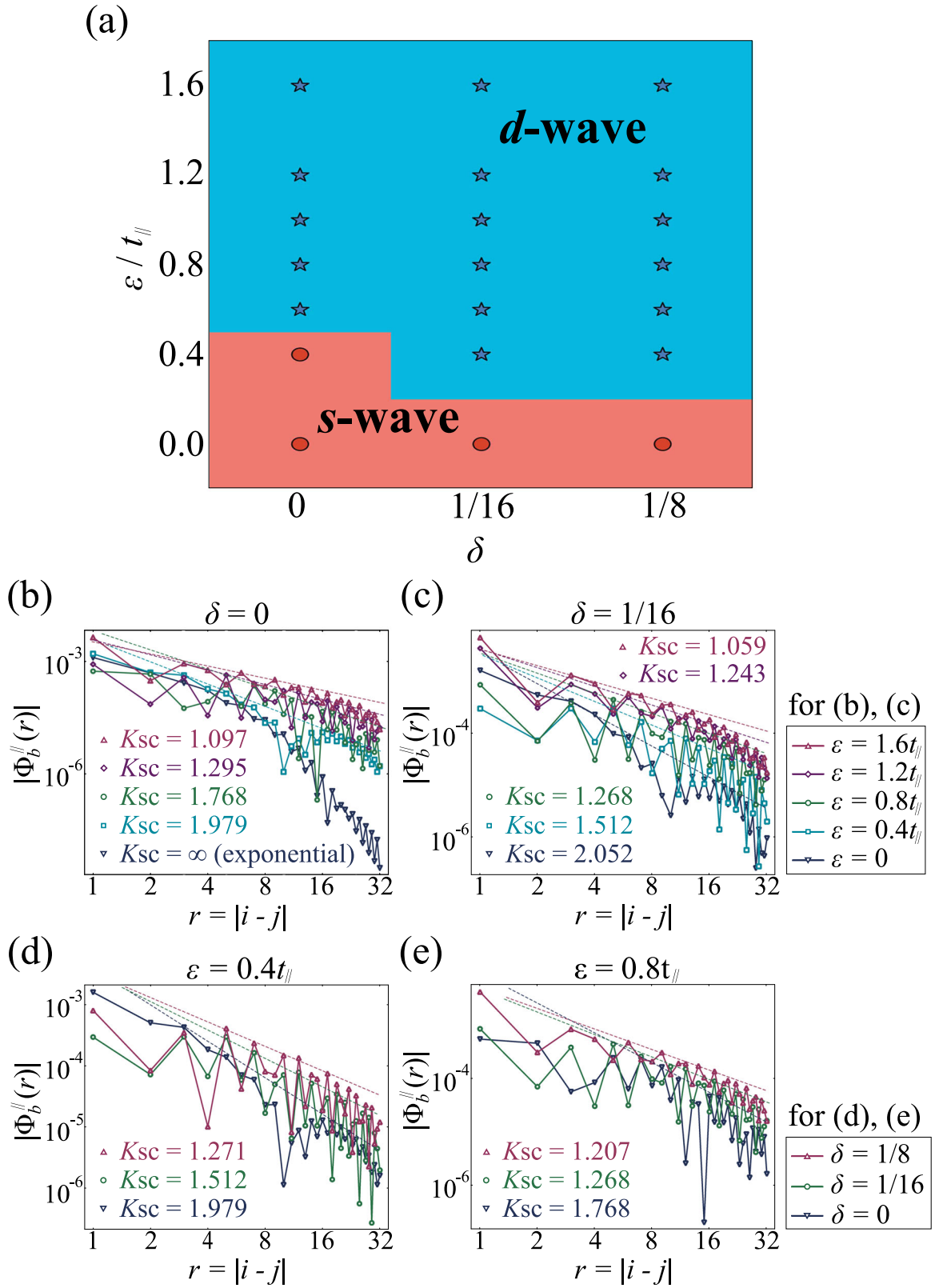

Fig. 4 | The DMRG results. a The $\delta - \varepsilon$ phase diagram of the ground state. The red region corresponds to the *s*-wave pairing and the blue region to the *d*-wave pairing. The absolute value of the intra-bottom-layer pairing correlation functions $|\Phi_b^{\parallel}(r)|$ under different electric fields $\varepsilon = 0, 0.4t_{\parallel}, 0.8t_{\parallel}, 1.2t_{\parallel}, 1.6t_{\parallel}$ for $\delta = 0$ in (**b**) and $\delta = 1/16$ in (**c**). $|\Phi_b^{\parallel}(r)|$ for different transferred $d_{x^2-y^2}$-electron-doping levels $\delta = 0, 1/16, 1/8$ under $\varepsilon = 0.4t_{\parallel}$ in (**d**) and $\varepsilon = 0.8t_{\parallel}$ in (**e**). The algebraic decay exponents K_{SC} are written in the four figures as well, reflecting the decay rate of the pairing correlation function with spatial distance, negatively correlated with the corresponding pairing strength. In (**a**–**e**), δ and ε are set as independent variables, since their exact relationship is unclear.

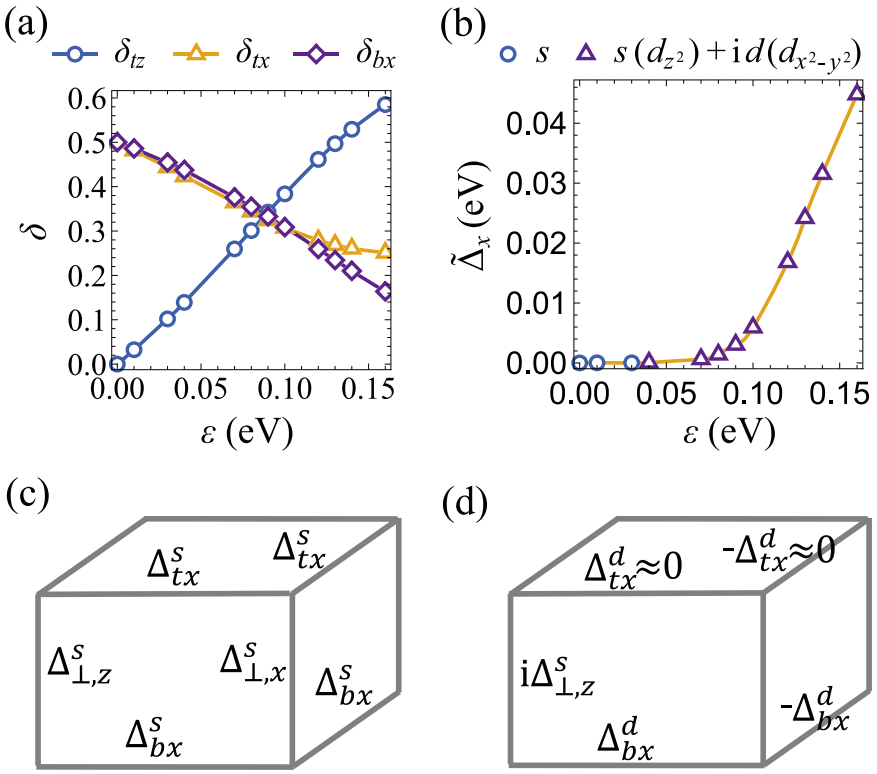

Fig. 5 | The SBMF results for the two-orbital model. a The hole densities $\delta_{i\mu\alpha}$ for the three orbitals as functions of the strength of the electric field ε. **b** The pairing gap amplitude of the bottom-layer $3d_{x^2-y^2}$-orbital as function of ε. **c**, **d** The pairing configurations of the *s*-wave and the $d(3d_{x^2-y^2})$+is$(3d_{z^2})$-wave, respectively.

The operators $c_{i\mu\alpha\sigma}$, $n_{i\mu\alpha}$, $\mathbf{S}_{i\mu\alpha}$ take the same meanings as those in model (1) except for an extra index $\alpha = x/z$ labeling the orbital, and $\widehat{P}$ is a projection operator projecting out the double occupancy in the same orbital of all sites. Note that $\mathbf{S}_{i\mu\alpha}$ for each orbital is spin-$\frac{1}{2}$ operator. ϵ_α denotes the on-site energy of the orbital α. We adpot the tight-binding (TB) parameters reported in ref. 141, i.e. $t_\parallel = 0.445$ eV, $t_{xz} = 0.221$ eV, $t_\perp = 0.503$ eV and $\epsilon_x - \epsilon_z = 0.367$ eV. The superexchange interactions are obtained through $J_\parallel \approx 4t_\parallel^2/U$ and $J_\perp \approx 4t_\perp^2/U$, with $U = 10t_\parallel$. Finally ε denotes the voltage between the two layers. Here, due to the weak super-exchange interaction between the d_{z^2} orbitals in the layer, we do not consider this term in our model. In addition, the Hund's coupling J_H of $La_3Ni_2O_7$ is generally considered to be in the range of 0.7 eV to 1 eV in past studies[68,70,76], which only slightly larger than the largest hopping parameter $t_\perp = 0.503$eV and thus does not satisfy the premise of the Schriffer-Wolf transformation or perturbation theory, we do not apply it here. More details are provided in *Methods*.

Our SBMF results of Eq. (2) (see *Methods* and the SI) are shown in Fig. 5. Figure 5(a) shows the ε-dependence of the hole densities $\delta_{i\mu\alpha}$. Obviously, the δ_{tz} enhances obviously with ε, suggesting that the top-$3d_{z^2}$ orbital is donating electrons. These donated electrons flow to the $3d_{x^2-y^2}$ orbitals in both layers, with more of them flowing to the bottom layer when $\varepsilon > 0.1$ eV while about half of them flow to the bottom layer when $\varepsilon \le 0.1$ eV. Figure 5(b) shows the ε-dependence of the pairing symmetry and the pairing gap amplitude of the bottom-layer $3d_{x^2-y^2}$ orbital. At low $\varepsilon \le 0.03$ eV, the pairing symmetry is *s*-wave, whose pairing configuration is shown in Fig. 5(c), wherein the $3d_{z^2}$-orbital form interlayer *s*-wave pseudo-gap, while the $3d_{x^2-y^2}$ orbital form *s*-wave SC with coexisting intralayer and interlayer pairing. In this regime the interlayer pairing is suppressed by the enhancement of ε while the intralayer pairing is enhanced. When $\varepsilon = 0$, the interlayer pairing gap is the largest. When ε is about 0.01 ~ 0.03 eV, the intralayer pairing gap is slightly larger than the interlayer pairing gap. When $\varepsilon > 0.03$ eV, the pairing symmetry is $d(3d_{x^2-y^2})$+is$(3d_{z^2})$, whose pairing configuration is shown in Fig. 5(d). In this state, the $3d_{z^2}$ orbital form interlayer *s*-wave pseudo-gap, while the bottom-layer $3d_{x^2-y^2}$ orbital form intralayer *d*-wave SC. When ε enhances in this regime, the pairing amplitude for the *d*-wave part enhances promptly. For $\varepsilon > 0.13$ eV, the pairing amplitude can go beyond 0.02 eV. Then from the relation $T_c \approx 0.42\widetilde{\Delta}$ for the *d*-wave SC illustrated in Fig. 3(b), we have got HTSC with $T_c \gtrsim 80$ K!

The result shown in Fig. 5(b) for the comprehensive two-orbital study and that shown in Fig. 3(b) for the simplified one-orbital study look similar, except that in Fig. 5(b) the result is expressed as function of the directly controllable quantity ε. Actually, if we replace the *x*-axis of Fig. 5(b) by the calculated $n_{bx} = 1 - \delta_{bx}$, the resulting curve nearly coincides with Fig. 3(b), particularly in the large-n_{bx} regime, see the SI. The main reason for such similarity lies in that under strong $\boldsymbol{\varepsilon}$, the dominant superconducting pairing is the intra-bottom-layer $3d_{x^2-y^2}$-orbital pairing, which is insensitive to the $3d_{z^2}$ orbital. The main new information obtained in the two-orbital study lies in that the $3d_{z^2}$ orbital form interlayer *s*-wave pseudo-gap which is mixed with the intra-bottom-layer *d*-wave HTSC of the $3d_{x^2-y^2}$ orbital in the ratio of 1: i, as shown in Fig. 5(d). This state breaks time-reversal symmetry, although the experimentally detected superconducting gap is the standard *d*-wave gap of the $3d_{x^2-y^2}$ orbital. This intriguing result is left for experimental verification.

Discussion

In conclusion, we propose that an imposed strong perpendicular electric field can drive HTSC with T_c above the boiling point of liquid nitrogen in the single-bilayer film of $La_3Ni_2O_7$ at AP. The reason lies in that under the strong electric field, the electrons in the layer with higher potential energy will flow to the layer with lower potential energy, to fill the $3d_{x^2-y^2}$ orbitals in the latter layer. When the imposed electric field is weak, it acts as the "pseudo-Zeeman field" operating on the layer index which supresses the interlayer SC, possibly inducing the PDW state. With considerably enhanced filling fraction, the $3d_{x^2-y^2}$ electrons in that layer just mimic the cuprates, which form

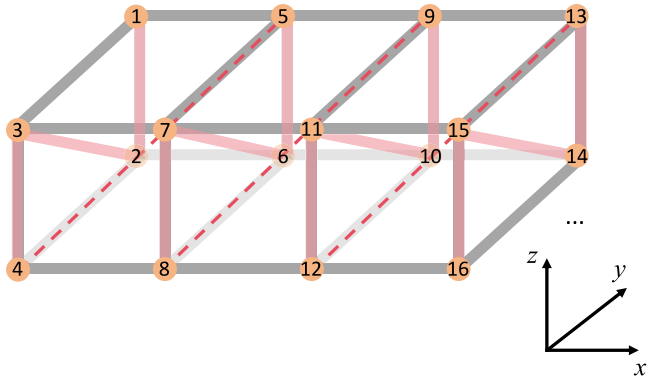

Fig. 6 | Illustration of the zigzag path in DMRG calculation.

intralayer *d*-wave HTSC with strongly enhanced T_c. Our combined one-orbital and two-orbital studies consistently verify this idea.

Presently, while different groups have provided slightly different TB parameters for the $La_3Ni_2O_7$ ultrathin film grown on SLAO substrate at AP, we have just adopted one set of these TB parameters to perform our calculations. However, the strong-coupling calculations performed here do not seriously rely on the accurate values of these parameters, because the main physics here is clear and simple. Actually, the well consistency between the result of the comprehensive two-orbital study and those of the simplified one-orbital studies with assuming different input conditions just verifies the robustness of our conclusion.

Moreover, we want to emphasize that the essence of introducing the perpendicular electric field is breaking the symmetry of the two layers by making their filling fractions different to each other. Actually, the filling fractions of different NiO layers in the $La_3Ni_2O_7$ ultrathin film grown on the SLAO substrate may different from each other because of the existence of the substrate on one side of the film. This can be considered as effective electric field. Thus, our work provides a possible way to understand the high T_c of the $La_3Ni_2O_7$ ultrathin film grown on the SLAO substrate.

Methods

The one-orbital model

The SBMF theory is used to solve the one-orbital model(1). In the SBMF approach, the superexchange terms are decomposed in $\chi-\Delta$ channel, e.g. $\mathbf{S}_{it}\cdot\mathbf{S}_{ib}=-\frac{3}{8}\left(\langle\chi^{\perp\dagger}\rangle\chi_i^{\perp}+\text{h.c.}+\langle\Delta^{\perp\dagger}\rangle\Delta_i^{\perp}+\text{h.c.}\right)$, χ and Δ represents hopping and pairing operators respectively. These MF parameters are further solved in a self-consistent manner. The specific steps can be referenced from prior work[79,107,156] and SI.

We also employ the DMRG method[157,158] to solve the ground state of the Hamiltonian(1) as a comparison for the SBMF approach. The tensor libraries TensorKit[159] and FiniteMPS[160] provide an implementation of the required symmetry[161,162]. We study the model on a $2\times2\times L_x$ lattice with the open boundary conditions in the x direction and choose $L_x=64$ for calculations. The matrix product state is constructed as shown in Fig. 6. We keep up to $D=12000$ $U(1)_{\text{charge}}\times SU(2)_{\text{spin}}$ multiplets in DMRG simulations and ensure the convergence accuracy of 10^{-6}.

The interlayer and intralayer singlet pairing operators take the form of

$$\begin{aligned}\Delta_i^{\perp\dagger}&=\tfrac{1}{\sqrt{2}}\left(c_{it\uparrow}^{\dagger}c_{ib\downarrow}^{\dagger}-c_{it\downarrow}^{\dagger}c_{ib\uparrow}^{\dagger}\right),\\ \Delta_{i\mu}^{\parallel\dagger}\equiv\Delta_{i\mu}^{\mathbf{x}\dagger}&=\tfrac{1}{\sqrt{2}}\left(c_{i\mu\uparrow}^{\dagger}c_{i+\mathbf{x},\mu\downarrow}^{\dagger}-c_{i\mu\downarrow}^{\dagger}c_{i+\mathbf{x},\mu\uparrow}^{\dagger}\right),\\ \Delta_{i\mu}^{\mathbf{y}\dagger}&=\tfrac{1}{\sqrt{2}}\left(c_{i\mu\uparrow}^{\dagger}c_{i+\mathbf{y},\mu\downarrow}^{\dagger}-c_{i\mu\downarrow}^{\dagger}c_{i+\mathbf{y},\mu\uparrow}^{\dagger}\right).\end{aligned}\tag{3}$$

Here, the subscripts $i+\mathbf{x}(i+\mathbf{y})$ represent the NN site of the site $\mathbf{i}$ in the $x(y)$ direction. Figure 7 shows how the singlet pairing operators are defined.

The considered correlation functions are defined as follow

$$\begin{aligned}\Phi^{\perp}(r)&=\left\langle\Delta_i^{\perp\dagger}\Delta_j^{\perp}\right\rangle,\\ \Phi_{\mu}^{\parallel}(r)\equiv\Phi_{\mu}^{\mathbf{xx}}(r)&=\left\langle\Delta_{i\mu}^{\parallel\dagger}\Delta_{j\mu}^{\parallel}\right\rangle,\\ \Phi_{\mu}^{\mathbf{xy}}(r)&=\left\langle\Delta_{i\mu}^{\parallel\dagger}\Delta_{j\mu}^{\mathbf{y}}\right\rangle,\end{aligned}\tag{4}$$

where $r=|\mathbf{i}-\mathbf{j}|$ is the distance between the sites i and j.

For a pairing channel whose absolute value of correlation function decays algebraically with distance, following the form $r^{-K_{\text{SC}}}$, the decay exponent K_{SC} is associated with the Luttinger parameter specific to the channel. $K_{SC}<2$ signals a divergent superconducting susceptibility in that channel. The channel with the lowest K_{SC} value is considered to dominate the pairing behavior.

The dominant pairing channel is related to pairing symmetry. For the case where interlayer pairing dominates, the pairing symmetry is restricted to *s*-wave pairing; while for the case where intralayer pairing in the bottom-layer dominates, we determine the pairing symmetry by the sign function $\text{sgn}\left[\Phi_b^{\parallel}(r)\Phi_b^{\mathbf{xy}}(r)\right]$. If $\text{sgn}\left[\Phi_b^{\parallel}(r)\Phi_b^{\mathbf{xy}}(r)\right]=-1$ holds for all r, the ground state can be identified as the *d*-wave pairing SC state. See SI for more details on DMRG.

The two-orbital model

Here we provide more technique details for the SBMF study on the two-orbital model(2). The electron operator is decomposed as $c_{i\mu\alpha\sigma}^{\dagger}=f_{i\mu\alpha\sigma}^{\dagger}b_{i\mu\alpha}$, where f is spinon operator and b is holon operator. Since we have found that $T_{\text{BEC}}\gg T_{\text{pair}}$ in the considered n_{bx} regime and T_{pair} is proportional to the zero-temperature spinon pairing gap, we can get the critical temperature of superconductivity only by calculating the ground-state spinon pairing gap. Thus we only consider the spinon Hamiltonian at zero temperature. The superexchange term is also decomposed in $\chi-\Delta$ channel. The spinon Hamiltonian is described as

$$\begin{aligned}H_{\text{spinon}}=&-t_{\parallel}\sum_{\langle i,j\rangle,\mu}\delta_{\mu x}\left(f_{i\mu x\sigma}^{\dagger}f_{j\mu x\sigma}+\text{h.c.}\right)\\ &-t_{xz}\sqrt{\delta_{tx}\delta_{tz}}\sum_{\langle i,j\rangle}\left(f_{itx\sigma}^{\dagger}f_{jtz\sigma}+f_{itz\sigma}^{\dagger}f_{jtx\sigma}+\text{h.c.}\right)\\ &-\tfrac{3}{8}J_{\parallel}\sum_{\langle i,j\rangle\mu}\left(\chi_{ij,\mu x}^{\dagger}\left\langle\chi_{\mu x}\right\rangle+\text{h.c.}-\left\langle\chi_{\mu x}^{\dagger}\right\rangle\left\langle\chi_{\mu x}\right\rangle\right)\\ &-\tfrac{3}{8}J_{\parallel}\sum_{\langle i,j\rangle\mu}\left(\Delta_{ij,\mu x}^{\dagger}\left\langle\Delta_{\mu x}\right\rangle+\text{h.c.}-\left\langle\Delta_{\mu x}^{\dagger}\right\rangle\left\langle\Delta_{\mu x}\right\rangle\right)\\ &-\tfrac{3}{8}J_{\perp}\sum_i\left(\chi_{iz}^{\perp\dagger}\langle\chi_z^{\perp}\rangle+\text{h.c.}-\left\langle\chi_z^{\perp\dagger}\right\rangle\langle\chi_z^{\perp}\rangle\right)\\ &-\tfrac{3}{8}J_{\perp}\sum_i\left(\Delta_{iz}^{\perp\dagger}\langle\Delta_z^{\perp}\rangle+\text{h.c.}-\left\langle\Delta_z^{\perp\dagger}\right\rangle\langle\Delta_z^{\perp}\rangle\right)\\ &-\tfrac{3}{8}\widetilde{J}_{\perp}\sum_i\left(\Delta_{ix}^{\perp\dagger}\langle\Delta_x^{\perp}\rangle+\text{h.c.}-\langle\Delta_x^{\perp\dagger}\rangle\langle\Delta_x^{\perp}\rangle\right)\\ &+\sum_{i\mu\alpha\sigma}\epsilon_{\alpha}n_{i\mu\alpha\sigma}+\tfrac{\varepsilon}{2}\sum_{ia\sigma}n_{it\alpha\sigma}-\tfrac{\varepsilon}{2}\sum_{ia\sigma}n_{ib\alpha\sigma}.\end{aligned}\tag{5}$$

where $\delta_{\mu\alpha}=\left\langle b_{i\mu\alpha}b_{j\mu\alpha}^{\dagger}\right\rangle$ since holon condense at zero temperature. Under the electric field, we have $\delta_{bz}=0$ and δ_{tz}, δ_{tx} and δ_{bx} are solved in a self-consistent manner by adjustment to onsite energies ϵ_{α} (See SI for more details). The mean-field order parameters are represented by

$$\begin{aligned}\chi_{ij,\mu x}&=\sum_{\sigma}f_{i\mu x\sigma}^{\dagger}f_{j\mu x\sigma},\\ \chi_{iz}^{\perp\dagger}&=\sum_{\sigma}f_{izt\sigma}^{\dagger}f_{izb\sigma},\\ \Delta_{ij,\mu\alpha}^{\dagger}&=f_{i\mu\alpha\uparrow}^{\dagger}f_{j\mu\alpha\downarrow}^{\dagger}-f_{i\mu\alpha\downarrow}^{\dagger}f_{j\mu\alpha\uparrow}^{\dagger},\\ \Delta_{ia}^{\perp\dagger}&=f_{it\alpha\uparrow}^{\dagger}f_{ib\alpha\downarrow}^{\dagger}-f_{ib\alpha\downarrow}^{\dagger}f_{it\alpha\uparrow}^{\dagger},\end{aligned}\tag{6}$$

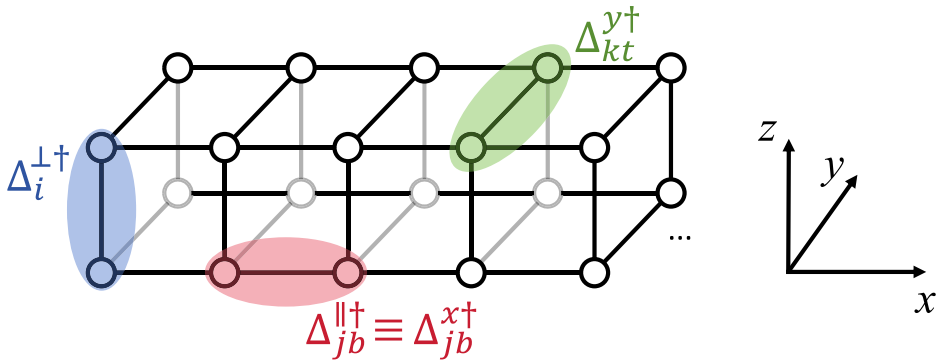

Fig. 7 | Illustration of the singlet pairing operators $\Delta_i^{\perp\dagger}$, $\Delta_{i\mu}^{\parallel\dagger}$ and $\Delta_{i\mu}^{\mathbf{y}\dagger}$.

and

$$\begin{aligned} \chi_{\mu x} &= \frac{1}{2N}\sum_{\langle i,j\rangle}\chi_{ij,\mu x},\ \chi_z^{\perp} = \frac{1}{N}\sum_i \chi_{iz}^{\perp}, \\ \Delta_{\mu x}^{\mathbf{x}} &= \frac{1}{2N}\sum_{\langle i,j\rangle}\Delta_{ij,\mu x},\ \Delta_{\alpha}^{\perp} = \frac{1}{N}\sum_i \Delta_{i\alpha}^{\perp}. \end{aligned} \tag{7}$$

Notably, the spin-exchange $\widetilde{J}_{\perp}$ of the Hamiltonian in Eq. (2) doesn't produce a hopping term $\chi_x^{\perp}$ in Eq. (5), which is the feature of such a bilayer system. Without interlayer hopping, a small interlayer spin-exchange $J_{\perp}$ leads to $\langle\chi^{\perp}\rangle \approx 0$.

Consequently, the $3d_{z^2}$ orbital only participate in the interlayer pairing. However, this pairing is not SC as the corresponding SC order parameter goes to zero in the SBMF theory due to $\delta_{bz} = 0$. The SC is carried by the $3d_{x^2-y^2}$ orbitals, which can form both intralayer and interlayer pairing. The superconducting T_c scales with the ground state gap amplitude of the $3d_{x^2-y^2}$ orbitals via the BCS relation exhibited in Fig. 3(b).

The expectation value of the mean-field order parameters are obtained by numerically solving the following self-consistent equations

$$\begin{aligned} \delta_{\mu\alpha} &= 1 - \frac{1}{N}\sum_k\left(\langle f_{k\mu\alpha\uparrow}^{\dagger} f_{k\mu\alpha\uparrow}\rangle + \langle f_{-k\mu\alpha\downarrow}^{\dagger} f_{-k\mu\alpha\downarrow}\rangle\right), \\ \delta_{tz} &= 0,\ \sum_{\mu\alpha}\delta_{\mu\alpha} \\ \langle\chi_{\mu x}\rangle &= \frac{1}{N}\sum_k \epsilon(\mathbf{k})\left(\langle f_{k\mu x\uparrow}^{\dagger} f_{k\mu x\uparrow}\rangle + \langle f_{-k\mu x\downarrow}^{\dagger} f_{-k\mu x\downarrow}\rangle\right), \\ \langle\chi_z^{\perp}\rangle &= \frac{1}{N}\sum_k\left(\langle f_{ktz\uparrow}^{\dagger} f_{kbz\uparrow}\rangle + \langle f_{-ktz\downarrow}^{\dagger} f_{-kbz\downarrow}\rangle\right), \\ \langle\Delta_{\mu x}^{\mathbf{x}}\rangle^{*} &= \frac{1}{N}\sum_k 2\cos(k_x)\langle f_{k\mu x\uparrow}^{\dagger} f_{-k\mu x\downarrow}^{\dagger}\rangle, \\ \langle\Delta_{\alpha}^{\perp}\rangle^{*} &= \frac{2}{N}\sum_k\langle f_{kt\alpha\uparrow}^{\dagger} f_{-kb\alpha\downarrow}^{\dagger}\rangle, \end{aligned} \tag{8}$$

where $\epsilon(\mathbf{k}) = \frac{\cos(k_x)+\cos(k_y)}{2}$.

Data availability

The data generated in this study have been deposited in the Zenodo database at https://zenodo.org/records/17691236.

Code availability

The code that supports the plots within this paper is available from the corresponding author upon request.

References

1. Sun, H. et al. Signatures of superconductivity near 80K in a nickelate under high pressure. *Nature* **621**, 493–498 (2023).
2. Zhang, Y. et al. High-temperature superconductivity with zero resistance and strange-metal behaviour in $La_3Ni_2O_{7-\delta}$. *Nat. Phys.* **20**, 1269–1273 (2024).
3. Hou, J. et al. Emergence of high-temperature superconducting phase in pressurized $La_3Ni_2O_7$ crystals. *Chin. Phys. Lett.* **40**, 117302 (2023).
4. Wang, G. et al. Pressure-induced superconductivity in polycrystalline $La_3Ni_2O_7$. *Phys. Rev. X* **14**, 011040 (2024).
5. Wang, G. et al. Observation of high-temperature superconductivity in the high-pressure tetragonal phase of $La_2PrNi_2O_{7-\delta}$. *arXiv:2311.08212*. https://arxiv.org/abs/2311.08212 (2023).
6. Zhang, M. et al. Effects of pressure and doping on Ruddlesden-Popper phases $La_{n+1}Ni_nO_{3n+1}$. *J. Mater. Sci. Technol.* **185**, 147–154 (2024).
7. Zhou, Y. et al. Investigations of key issues on the reproducibility of high-T_c superconductivity emerging from compressed $La_3Ni_2O_7$. *Matter Radiat. Extrem.* **10**, 027801 (2025).
8. Wang, N. et al. Bulk high-temperature superconductivity in the high-pressure tetragonal phase of bilayer $La_2PrNi_2O_7$. *Nature* **634**, 579–584 (2024).
9. Li, J. et al. Identification of the superconductivity in bilayer nickelate $La_3Ni_2O_7$ upon 100 gpa. *Natl. Sci. Rev.* **12**, nwaf220 (2025).
10. Fukamachi, T., Kobayashi, Y., Miyashita, T. & Sato, M. ^{139}La NMR studies of layered perovskite systems $La_3Ni_2O_{7-\delta}$ and $La_4Ni_3O_{10}$. *J. Phys. Chem. Solids* **62**, 195–198 (2001).
11. Khasanov, R. et al. Pressure-enhanced splitting of density wave transitions in $La_3Ni_2O_{7-\delta}$. *Nat. Phys.* **21**, 430–436 (2025).
12. Chen, K. et al. Evidence of spin density waves in $La_3Ni_2O_{7-\delta}$. *Phys. Rev. Lett.* **132**, 256503 (2024).
13. Zhao, D. et al. Pressure-enhanced spin-density-wave transition in double-layer nickelate $La_3Ni_2O_{7-\delta}$. *Sci. Bull.* **70**, 1239–1245 (2025).
14. Chen, X. et al. Electronic and magnetic excitations in $La_3Ni_2O_7$. *Nat. Commun.* **15**, 9597 (2024).
15. Liu, Z. et al. Evidence for charge and spin density waves in single crystals of $La_3Ni_2O_7$ and $La_3Ni_2O_6$. *Sci. China-Phys. Mech. Astron.* **66**, 217411 (2023).
16. Kakoi, M. et al. Multiband metallic ground state in multilayered nickelates $La_3Ni_2O_7$ and $La_4Ni_3O_{10}$ probed by ^{139}La-NMR at ambient pressure. *J. Phys. Soc. Jpn.* **93**, 053702 (2024).
17. Xie, T. et al. Strong interlayer magnetic exchange coupling in $La_3Ni_2O_{7-\delta}$ revealed by inelastic neutron scattering. *Sci. Bull.* **69**, 3221–3227 (2024).
18. Gupta, N. K. et al. Anisotropic spin stripe domains in bilayer $La_3Ni_2O_7$. *Nat. Commun.* **16**, 6560 (2025).
19. Ren, X. et al. Resolving the electronic ground state of $La_3Ni_2O_{7-\delta}$ films. *Commun. Phys.* **8**, 52 (2025).
20. Feng, J.-J. et al. Unaltered density wave transition and pressure-induced signature of superconductivity in Nd-doped $La_3Ni_2O_7$. *Phys. Rev. B* **110**, L100507 (2024).

21. Meng, Y. et al. Density-wave-like gap evolution in $La_3Ni_2O_7$ under high pressure revealed by ultrafast optical spectroscopy. *Nat. Commun.* **15**, 10408 (2024).
22. Fan, S. et al. Tunneling spectra with gaplike features observed in nickelate $La_3Ni_2O_7$ at ambient pressure. *Phys. Rev. B* **110**, 134520 (2024).
23. Xu, M. et al. Pressure-induced phase transitions in bilayer $La_3Ni_2O_7$. *J. Phys. Chem. C*. https://doi.org/10.1021/acs.jpcc.5c07252 (2025).
24. Li, Y. et al. Distinct ultrafast dynamics of bilayer and trilayer nickelate superconductors regarding the density-wave-like transitions. *Sci. Bull*. https://www.sciencedirect.com/science/article/pii/S2095927324007503 (2024).
25. Liu, Z. et al. Electronic correlations and partial gap in the bilayer nickelate $La_3Ni_2O_7$. *Nat. Commun.* **15**, 7570 (2024).
26. Yashima, M. et al. Microscopic evidence for spin–spinless stripe order with reduced Ni moments within *ab* plane for bilayer nickelate $La_3Ni_2O_7$ probed by ^{139}La-NQR. *J. Phys. Soc. Jpn.* **94**, 054704 (2025).
27. Khasanov, R. et al. Oxygen-isotope effect on the density wave transitions in $La_3Ni_2O_7$ and $La_4Ni_3O_{10}$. *arXiv:2504.08290*. https://arxiv.org/abs/2504.08290 (2025).
28. Yang, J. et al. Orbital-dependent electron correlation in double-layer nickelate $La_3Ni_2O_7$. *Nat. Commun.* **15**, 4373 (2024).
29. Wang, L. et al. Structure responsible for the superconducting state in $La_3Ni_2O_7$ at low temperature and high pressure conditions. *J. Am. Chem. Soc.* **146**, 7506–7514 (2024).
30. Cui, T. et al. Strain mediated phase crossover in Ruddlesden Popper nickelates. *Commun. Mater.* **5**, 32 (2024).
31. Li, Y. et al. Electronic correlation and pseudogap-like behavior of high-temperature superconductor $La_3Ni_2O_7$. *Chin. Phys. Lett.* **41**, 087402 (2024).
32. Li, M. et al. Distinguishing electronic band structure of single-layer and bilayer Ruddlesden-Popper nickelates probed by in-situ high pressure X-ray absorption near-edge spectroscopy. *arXiv:2410.04230*. https://arxiv.org/abs/2410.04230 (2024).
33. Zhou, X. et al. Revealing nanoscale structural phase separation in $La_3Ni_2O_{7-\delta}$ single crystal via scanning near-field optical microscopy. *arXiv:2410.06602*. https://arxiv.org/abs/2410.06602 (2024).
34. Wang, G. et al. Chemical versus physical pressure effects on the structure transition of bilayer nickelates. *npj Quantum Mater.* **10**, 1 (2025).
35. Chen, X. et al. Polymorphism in the Ruddlesden–Popper nickelate $La_3Ni_2O_7$: discovery of a hidden phase with distinctive layer stacking. *J. Am. Chem. Soc.* **146**, 3640–3645 (2024).
36. Dong, Z. et al. Visualization of oxygen vacancies and self-doped ligand holes in $La_3Ni_2O_{7-\delta}$. *Nature* **630**, 847–852 (2024).
37. Li, F. et al. Design and synthesis of three-dimensional hybrid Ruddlesden-Popper nickelate single crystals. *Phys. Rev. Mater.* **8**, 053401 (2024).
38. Puphal, P. et al. Unconventional crystal structure of the high-pressure superconductor $La_3Ni_2O_7$. *Phys. Rev. Lett.* **133**, 146002 (2024).
39. Zhu, Y. et al. Superconductivity in pressurized trilayer $La_4Ni_3O_{10-\delta}$ single crystals. *Nature* **631**, 531–536 (2024).
40. Zhang, M. et al. Superconductivity in trilayer nickelate $La_4Ni_3O_{10}$ under pressure. *Phys. Rev. X* **15**, 021005 (2025).
41. Huang, X. et al. Signature of superconductivity in pressurized trilayer-nickelate $Pr_4Ni_3O_{10-\delta}$. *Chin. Phys. Lett.* **41**, 127403 (2024).
42. Li, Q. et al. Signature of superconductivity in pressurized $La_4Ni_3O_{10}$. *Chin. Phys. Lett.* **41**, 017401 (2024).
43. Zhang, J. et al. Intertwined density waves in a metallic nickelate. *Nat. Commun.* **11**, 6003 (2020).
44. Xu, S. et al. Origin of the density wave instability in trilayer nickelate $La_4Ni_3O_{10}$ revealed by optical and ultrafast spectroscopy. *Phys. Rev. B* **111**, 075140 (2025).
45. Du, X. et al. Correlated electronic structure and density-wave gap in trilayer nickelate $La_4Ni_3O_{10}$. *arXiv:2405.19853*. https://arxiv.org/abs/2405.19853 (2024).
46. Li, D. et al. Superconductivity in an infinite-layer nickelate. *Nature* **572**, 624–627 (2019).
47. Lee, K. et al. Linear-in-temperature resistivity for optimally superconducting (Nd, Sr) NiO_2. *Nature* **619**, 288–292 (2023).
48. Nomura, Y. & Arita, R. Superconductivity in infinite-layer nickelates. *Rep. Prog. Phys.* **85**, 052501 (2022).
49. Gu, Q. & Wen, H.-H. Superconductivity in nickel-based 112 systems. *Innovation* **3**. https://www.cell.com/the-innovation/fulltext/S2666-6758(21)00127-2 (2022).
50. Sui, X. et al. Electronic properties of the bilayer nickelates $R_3Ni_2O_7$ with oxygen vacancies (R = La or Ce). *Phys. Rev. B* **109**, 205156 (2024).
51. Luo, Z., Hu, X., Wang, M., Wú, W. & Yao, D.-X. Bilayer two-orbital model of $La_3Ni_2O_7$ under pressure. *Phys. Rev. Lett.* **131**, 126001 (2023).
52. Zhang, Y., Lin, L.-F., Moreo, A. & Dagotto, E. Electronic structure, dimer physics, orbital-selective behavior, and magnetic tendencies in the bilayer nickelate superconductor $La_3Ni_2O_7$ under pressure. *Phys. Rev. B* **108**, L180510 (2023).
53. Cao, Y. & Yang, Y. -f. Flat bands promoted by Hund's rule coupling in the candidate double-layer high-temperature superconductor $La_3Ni_2O_7$ under high pressure. *Phys. Rev. B* **109**, L081105 (2024).
54. Zhang, Y., Lin, L.-F., Moreo, A., Maier, T. A. & Dagotto, E. Structural phase transition, $s_\pm$-wave pairing, and magnetic stripe order in bilayered superconductor $La_3Ni_2O_7$ under pressure. *Nat. Commun.* **15**, 2470 (2024).
55. Huang, J., Wang, Z. D. & Zhou, T. Impurity and vortex states in the bilayer high-temperature superconductor $La_3Ni_2O_7$. *Phys. Rev. B* **108**, 174501 (2023).
56. Geisler, B., Hamlin, J. J., Stewart, G. R., Hennig, R. G. & Hirschfeld, P. Structural transitions, octahedral rotations, and electronic properties of $A_3Ni_2O_7$ rare-earth nickelates under high pressure. *npj Quantum Mater.* **9**, 38 (2024).
57. Rhodes, L. C. & Wahl, P. Structural routes to stabilize superconducting $La_3Ni_2O_7$ at ambient pressure. *Phys. Rev. Mater.* **8**, 044801 (2024).
58. Zhang, Y., Lin, L.-F., Moreo, A., Maier, T. A. & Dagotto, E. Electronic structure, magnetic correlations, and superconducting pairing in the reduced Ruddlesden-Popper bilayer $La_3Ni_2O_6$ under pressure: Different role of $d_{3z^2-r^2}$ orbital compared with $La_3Ni_2O_7$. *Phys. Rev. B*. **109**, 045151 (2024).
59. Yuan, N., Elghandour, A., Arneth, J., Dey, K. & Klingeler, R. High-pressure crystal growth and investigation of the metal-to-metal transition of Ruddlesden-Popper trilayer nickelates $La_4Ni_3O_{10}$. *J. Cryst. Growth* **627**, 127511 (2024).
60. Li, J. et al. Structural transition, electric transport, and electronic structures in the compressed trilayer nickelate $La_4Ni_3O_{10}$. *Sci. China Phys. Mech. Astron.* **67**, 117403 (2024).
61. Geisler, B. et al. Optical properties and electronic correlations in $La_3Ni_2O_{7-\delta}$ bilayer nickelates under high pressure. *npj Quantum Mater.* **9**, 89 (2024).
62. Li, H. et al. Fermiology and electron dynamics of trilayer nickelate $La_4Ni_3O_{10}$. *Nat. Commun.* **8**, 704 (2017).
63. Wang, J.-X., Ouyang, Z., He, R.-Q. & Lu, Z.-Y. Non-Fermi liquid and Hund correlation in $La_4Ni_3O_{10}$ under high pressure. *Phys. Rev. B* **109**, 165140 (2024).
64. Chen, C.-Q., Luo, Z., Wang, M., Wú, W. & Yao, D.-X. Trilayer multiorbital models of $La_4Ni_3O_{10}$. *Phys. Rev. B* **110**, 014503 (2024).

65. Shen, Y., Qin, M. & Zhang, G.-M. Effective bi-layer model hamiltonian and density-matrix renormalization group study for the high-T_c superconductivity $La_3Ni_2O_7$ under high pressure. *Chin. Phys. Lett.* **40**, 127401 (2023).
66. Christiansson, V., Petocchi, F. & Werner, P. Correlated electronic structure of $La_3Ni_2O_7$ under pressure. *Phys. Rev. Lett.* **131**, 206501 (2023).
67. Shilenko, D. A. & Leonov, I. V. Correlated electronic structure, orbital-selective behavior, and magnetic correlations in double-layer $La_3Ni_2O_7$ under pressure. *Phys. Rev. B* **108**, 125105 (2023).
68. Wú, W., Luo, Z., Yao, D.-X. & Wang, M. Superexchange and charge transfer in the nickelate superconductor $La_3Ni_2O_7$ under pressure. *Sci. China-Phys. Mech. Astron.* **67**, 117402 (2024).
69. Chen, X., Jiang, P., Li, J., Zhong, Z. & Lu, Y. Charge and spin instabilities in superconducting $La_3Ni_2O_7$. *Phys. Rev. B* **111**, 014515 (2025).
70. Ouyang, Z. et al. Hund electronic correlation in $La_3Ni_2O_7$ under high pressure. *Phys. Rev. B* **109**, 115114 (2024).
71. Heier, G., Park, K. & Savrasov, S. Y. Competing d_{xy} and $s_\pm$ pairing symmetries in superconducting $La_3Ni_2O_7$: LDA + FLEX calculations. *Phys. Rev. B* **109**, 104508 (2024).
72. Wang, Y., Jiang, K., Wang, Z., Zhang, F.-C. & Hu, J. Electronic and magnetic structures of bilayer $La_3Ni_2O_7$ at ambient pressure. *Phys. Rev. B* **110**, 205122 (2024).
73. Bötzel, S., Lechermann, F., Gondolf, J. & Eremin, I. M. Theory of magnetic excitations in multilayer nickelate superconductor $La_3Ni_2O_7$. *Phys. Rev. B* **109**, L180502 (2024).
74. Yang, Q.-G., Wang, D. & Wang, Q.-H. Possible $S_\pm$-wave superconductivity in $La_3Ni_2O_7$. *Phys. Rev. B* **108**, L140505 (2023).
75. Liu, Y.-B., Mei, J.-W., Ye, F., Chen, W.-Q. & Yang, F. $s^\pm$-wave pairing and the destructive role of apical-oxygen deficiencies in $La_3Ni_2O_7$ under pressure. *Phys. Rev. Lett.* **131**, 236002 (2023).
76. Lechermann, F., Gondolf, J., Bötzel, S. & Eremin, I. M. Electronic correlations and superconducting instability in $La_3Ni_2O_7$ under high pressure. *Phys. Rev. B* **108**, L201121 (2023).
77. Sakakibara, H., Kitamine, N., Ochi, M. & Kuroki, K. Possible high T_c superconductivity in $La_3Ni_2O_7$ under high pressure through manifestation of a nearly half-filled bilayer Hubbard model. *Phys. Rev. Lett.* **132**, 106002 (2024).
78. Gu, Y., Le, C., Yang, Z., Wu, X. & Hu, J. Effective model and pairing tendency in the bilayer Ni-based superconductor $La_3Ni_2O_7$. *Phys. Rev. B* **111**, 174506 (2025).
79. Lu, C., Pan, Z., Yang, F. & Wu, C. Interlayer-coupling-driven high-temperature superconductivity in $La_3Ni_2O_7$ under pressure. *Phys. Rev. Lett.* **132**, 146002 (2024).
80. Oh, H. & Zhang, Y.-H. Type-II *t-J* model and shared superexchange coupling from Hund's rule in superconducting $La_3Ni_2O_7$. *Phys. Rev. B* **108**, 174511 (2023).
81. Liao, Z. et al. Electron correlations and superconductivity in $La_3Ni_2O_7$ under pressure tuning. *Phys. Rev. B* **108**, 214522 (2023).
82. Qu, X.-Z. et al. Bilayer *t-J-*$J_\perp$ model and magnetically mediated pairing in the pressurized nickelate $La_3Ni_2O_7$. *Phys. Rev. Lett.* **132**, 036502 (2024).
83. Yang, Y.-F., Zhang, G.-M. & Zhang, F.-C. Interlayer valence bonds and two-component theory for high-T_c superconductivity of $La_3Ni_2O_7$ under pressure. *Phys. Rev. B* **108**, L201108 (2023).
84. Jiang, K., Wang, Z. & Zhang, F.-C. High temperature superconductivity in $La_3Ni_2O_7$. *Chin. Phys. Lett.* **41**, 017402 (2024).
85. Zhang, Y., Lin, L.-F., Moreo, A., Maier, T. A. & Dagotto, E. Trends in electronic structures and $s_\pm$-wave pairing for the rare-earth series in bilayer nickelate superconductor $R_3Ni_2O_7$. *Phys. Rev. B* **108**, 165141 (2023).
86. Qin, Q. & Yang, Y.-F. High-T_c superconductivity by mobilizing local spin singlets and possible route to higher T_c in pressurized $La_3Ni_2O_7$. *Phys. Rev. B.* **108**, L140504 (2023).
87. Tian, Y.-H., Chen, Y., Wang, J.-M., He, R.-Q. & Lu, Z.-Y. Correlation effects and concomitant two-orbital $s_\pm$-wave superconductivity in $La_3Ni_2O_7$ under high pressure. *Phys. Rev. B* **109**, 165154 (2024).
88. Jiang, R., Hou, J., Fan, Z., Lang, Z.-J. & Ku, W. Pressure driven fractionalization of ionic spins results in cupratelike high-T_c superconductivity in $La_3Ni_2O_7$. *Phys. Rev. Lett.* **132**, 126503 (2024).
89. Lu, D.-C. et al. Superconductivity from doping symmetric mass generation insulators: Application to $La_3Ni_2O_7$ under pressure. *arXiv:2308.11195*. https://arxiv.org/abs/2308.11195 (2023).
90. Kitamine, N., Ochi, M. & Kuroki, K. Theoretical designing of multi-band nickelate and palladate superconductors with $d^{8+\delta}$ configuration. *arXiv:2308.12750*. https://arxiv.org/abs/2308.12750 (2023).
91. Luo, Z., Lv, B., Wang, M., Wú, W. & Yao, D.-X. High-T_c superconductivity in $La_3Ni_2O_7$ based on the bilayer two-orbital t-J model. *npj Quantum Mater.* **9**, 61 (2024).
92. Zhang, J.-X., Zhang, H.-K., You, Y.-Z. & Weng, Z.-Y. Strong pairing originated from an emergent $\mathbb{Z}_2$ berry phase in $La_3Ni_2O_7$. *Phys. Rev. Lett.* **133**, 126501 (2024).
93. Pan, Z., Lu, C., Yang, F. & Wu, C. Effect of rare-earth element substitution in superconducting $R_3Ni_2O_7$ under pressure. *Chin. Phys. Lett.* **41**, 087401 (2024).
94. Sakakibara, H. et al. Theoretical analysis on the possibility of superconductivity in the trilayer Ruddlesden-Popper nickelate $La_4Ni_3O_{10}$ under pressure and its experimental examination: Comparison with $La_3Ni_2O_7$. *Phys. Rev. B* **109**, 144511 (2024).
95. Lange, H. et al. Pairing dome from an emergent Feshbach resonance in a strongly repulsive bilayer model. *Phys. Rev. B* **110**, L081113 (2024).
96. Yang, H., Oh, H. & Zhang, Y.-H. Strong pairing from a small Fermi surface beyond weak coupling: Application to $La_3Ni_2O_7$. *Phys. Rev. B* **110**, 104517 (2024).
97. Lange, H. et al. Feshbach resonance in a strongly repulsive ladder of mixed dimensionality: A possible scenario for bilayer nickelate superconductors. *Phys. Rev. B* **109**, 045127 (2024).
98. Kaneko, T., Sakakibara, H., Ochi, M. & Kuroki, K. Pair correlations in the two-orbital Hubbard ladder: Implications for superconductivity in the bilayer nickelate $La_3Ni_2O_7$. *Phys. Rev. B* **109**, 045154 (2024).
99. Fan, Z. et al. Superconductivity in nickelate and cuprate superconductors with strong bilayer coupling. *Phys. Rev. B* **110**, 024514 (2024).
100. Wu, X., Yang, H. & Zhang, Y.-H. Deconfined Fermi liquid to Fermi liquid transition and superconducting instability. *Phys. Rev. B* **110**, 125122 (2024).
101. Zhang, Y., Lin, L.-F., Moreo, A., Maier, T. A. & Dagotto, E. Prediction of $s^\pm$-wave superconductivity enhanced by electronic doping in trilayer nickelates $La_4Ni_3O_{10}$ under pressure. *Phys. Rev. Lett.* **133**, 136001 (2024).
102. Zhang, M. et al. The $s^\pm$-wave superconductivity in the pressurized $La_4Ni_3O_{10}$. *Phys. Rev. B* **110**, L180501 (2024).
103. Yang, Q.-G., Jiang, K.-Y., Wang, D., Lu, H.-Y. & Wang, Q.-H. Effective model and $s_\pm$-wave superconductivity in trilayer nickelate $La_4Ni_3O_{10}$. *Phys. Rev. B* **109**, L220506 (2024).
104. Zhang, Y., Lin, L.-F., Moreo, A., Maier, T. A. & Dagotto, E. Electronic structure, self-doping, and superconducting instability in the alternating single-layer trilayer stacking nickelates $La_3Ni_2O_7$. *Phys. Rev. B* **110**, L060510 (2024).
105. Yang, Y.-F. Decomposition of multilayer superconductivity with interlayer pairing. *Phys. Rev. B* **110**, 104507 (2024).
106. Ryee, S., Witt, N. & Wehling, T. O. Quenched pair breaking by interlayer correlations as a key to superconductivity in $La_3Ni_2O_7$. *Phys. Rev. Lett.* **133**, 096002 (2024).
107. Lu, C., Pan, Z., Yang, F. & Wu, C. Interplay of two E_g orbitals in superconducting $La_3Ni_2O_7$ under pressure. *Phys. Rev. B* **110**, 094509 (2024).

108. Ouyang, Z., Gao, M. & Lu, Z.-Y. Absence of electron-phonon coupling superconductivity in the bilayer phase of $La_3Ni_2O_7$ under pressure. *npj Quantum Mater.* **9**, 80 (2024).
109. LaBollita, H., Pardo, V., Norman, M. R. & Botana, A. S. Electronic structure and magnetic properties of $La_3Ni_2O_7$ under pressure: active role of the Ni-$d_{x^2-y^2}$ orbitals. *arXiv:2309.17279*. https://arxiv.org/abs/2309.17279 (2024).
110. Zhang, B., Xu, C. & Xiang, H. Emergent spin-charge-orbital order in superconductor $La_3Ni_2O_7$. *arXiv:2407.18473*. https://arxiv.org/abs/2407.18473 (2024).
111. Leonov, I. V. Electronic correlations and spin-charge-density stripes in double-layer $La_3Ni_2O_7$. *arXiv:2410.15298*. https://arxiv.org/abs/2410.15298v1 (2024).
112. LaBollita, H., Pardo, V., Norman, M. R. & Botana, A. S. Assessing spin-density wave formation in $La_3Ni_2O_7$ from electronic structure calculations. *Phys. Rev. Mater.* **8**, L111801 (2024).
113. Ni, X.-S. et al. Spin density wave in the bilayered nickelate $La_3Ni_2O_{7-\delta}$ at ambient pressure. *npj Quantum Mater.* **10**, 17 (2025).
114. Yi, X.-W. et al. Nature of charge density waves and metal-insulator transition in pressurized $La_3Ni_2O_7$. *Phys. Rev. B* **110**, L140508 (2024).
115. LaBollita, H., Kapeghian, J., Norman, M. R. & Botana, A. S. Electronic structure and magnetic tendencies of trilayer $La_4Ni_3O_{10}$ under pressure: Structural transition, molecular orbitals, and layer differentiation. *Phys. Rev. B* **109**, 195151 (2024).
116. Jiang, K.-Y., Cao, Y.-H., Yang, Q.-G., Lu, H.-Y. & Wang, Q.-H. Theory of pressure dependence of superconductivity in bilayer nickelate $La_3Ni_2O_7$. *Phys. Rev. Lett.* **134**, 076001 (2025).
117. Chen, Y., Tian, Y.-H., Wang, J.-M., He, R.-Q. & Lu, Z.-Y. Non-Fermi liquid and antiferromagnetic correlations with hole doping in the bilayer two-orbital Hubbard model of $La_3Ni_2O_7$ at zero temperature. *Phys. Rev. B* **110**, 235119 (2024).
118. Zhang, Y., Lin, L.-F., Moreo, A., Maier, T. A., & Dagotto, E. Magnetic correlations and pairing tendencies of the hybrid stacking nickelate superlattice $La_7Ni_5O_{17}$ ($La_3Ni_2O_7$/$La_4Ni_3O_{10}$) under pressure. *Phys. Rev. B* **112**, 024508 (2025).
119. Lin, L.-F. et al. Magnetic phase diagram of a two-orbital model for bilayer nickelates with varying doping. *Phys. Rev. B* **110**, 195135 (2024).
120. Jiang, G. et al. Intertwined charge and spin instability of $La_3Ni_2O_7$. *Sci. China-Phys. Mech. Astron.* **68**, 297411 (2025).
121. Leonov, I. V. Electronic structure and magnetic correlations in the trilayer nickelate superconductor $La_4Ni_3O_{10}$ under pressure. *Phys. Rev. B* **109**, 235123 (2024).
122. Liu, Y. et al. Growth and characterization of the $La_3Ni_2O_{7-\delta}$ thin films: dominant contribution of the $d_{x^2-y^2}$ orbital at ambient pressure. *Phys. Rev. Mater.* **8**, 124801 (2024).
123. Liu, Y. Ou, M., Wang, Y. & Wen, H.-H. Temperature-independent Hall coefficient in hole-doped $La_3Ni_2O_7$ thin films: evidence for single-band transport. *J. Phys.: Condens. Matter* **37**, 255502 (2025).
124. Tian, Y. & Chen, Y. Spin density wave and superconductivity in the bilayer *t-J* model of $La_3Ni_2O_7$ under renormalized mean-field theory. *Phys. Rev. B* **112**, 014520 (2025).
125. Yin, Y., Zhan, J., Liu, B. & Han, X. The *s* ± pairing symmetry in the pressured $La_3Ni_2O_7$ from electron-phonon coupling. *arXiv:2502.21016*. https://arxiv.org/abs/2502.21016 (2025).
126. Xi, W., Yu, S.-L. & Li, J.-X. Transition from $s_{\pm}$-wave to $d_{x^2-y^2}$-wave superconductivity driven by interlayer interaction in the bilayer two-orbital model of $La_3Ni_2O_7$. *Phys. Rev. B* **111**, 104505 (2025).
127. Kaneko, T., Kakoi, M. & Kuroki, K. *t-J* model for strongly correlated two-orbital systems: Application to bilayer nickelate superconductors. *Phys. Rev. B* **112**, 075143 (2025).
128. Ji, J.-H. et al. A strong-coupling-limit study on the pairing mechanism in the pressurized $La_3Ni_2O_7$. *arxiv:2504.12127*. https://arxiv.org/abs/2504.12127 (2025).
129. Wang, Y., Zhang, Y. & Jiang, K. Electronic structure and disorder effect of $La_3Ni_2O_7$ superconductor. *Chin. Phys. B* **34**, 047105 (2025).
130. Haque, M. E., Ali, R., Masum, M., Hassan, J. & Naqib, S. DFT exploration of pressure dependent physical properties of the recently discovered $La_3Ni_2O_7$ superconductor. *arXiv:2504.15853*. https://arxiv.org/abs/2504.15853 (2025).
131. Shi, L., Luo, Y., Wu, W. & Zhang, Y. Theoretical investigation of high-T_c superconductivity in Sr-doped $La_3Ni_2O_7$ at ambient pressure. *arXiv:2503.13197*. https://arxiv.org/abs/2503.13197 (2025).
132. Ko, E. K. et al. Signatures of ambient pressure superconductivity in thin film $La_3Ni_2O_7$. *Nature* **638**, 935–940 (2025).
133. Zhou, G. et al. Ambient-pressure superconductivity onset above 40 K in (La, Pr)$_3Ni_2O_7$ films. *Nature* **640**, 641–646 (2025).
134. Liu, Y. et al. Superconductivity and normal-state transport in compressively strained $La_2PrNi_2O_7$ thin films. *Nat. Mater.* **24**, 1221–1227 (2025).
135. Yue, C. et al. Correlated electronic structures and unconventional superconductivity in bilayer nickelate heterostructures. *Natl. Sci. Rev.* **12**, nwaf253 (2025).
136. Li, P. et al. Angle-resolved photoemission spectroscopy of superconducting (La,Pr)$_3Ni_2O_7$/$SrLaAlO_4$ heterostructures. *Natl. Sci. Rev.* **12**, nwaf205 (2025).
137. Bhatt, L. et al. Resolving structural origins for superconductivity in strain-engineered $La_3Ni_2O_7$ thin films. *arXiv:2501.08204*. https://arxiv.org/abs/2501.08204 (2025).
138. Shao, Z.-Y., Liu, Y.-B., Liu, M. & Yang, F. Band structure and pairing nature of $La_3Ni_2O_7$ thin film at ambient pressure. *Phys. Rev. B* **112**, 024506 (2025).
139. Shi, H. et al. The effect of carrier doping and thickness on the electronic structures of $La_3Ni_2O_7$ thin films. *Chin. Phys. Lett.* **42**, 080708 (2025).
140. Le, C., Zhan, J., Wu, X. & Hu, J. Landscape of correlated orders in strained bilayer nickelate thin films. *arXiv:2501.14665*. https://arxiv.org/abs/2501.14665 (2025).
141. Hu, X., Qiu, W., Chen, C.-Q., Luo, Z. & Yao, D.-X. Electronic structures and multi-orbital models of $La_3Ni_2O_7$ thin films at ambient pressure. *Commun. Phys.* https://doi.org/10.1038/s42005-025-02411-8 (2025).
142. Wang, B. Y. et al. Electronic structure of compressively strained thin film $La_2PrNi_2O_7$. *arxiv:2504.16372*. https://arxiv.org/abs/2504.16372 (2025).
143. Huang, J. & Zhou, T. Effective perpendicular electric field as a probe for interlayer pairing in ambient-pressure superconducting $La_{2.85}Pr_{0.15}Ni_2O_7$ thin films. *Phys. Rev. B* **112**, 054506 (2025).
144. Geisler, B., Hamlin, J. J., Stewart, G. R., Hennig, R. G. & Hirschfeld, P. Electronic reconstruction and interface engineering of emergent spin fluctuations in compressively strained $La_3Ni_2O_7$ on $SrLaAlO_4$(001). *arXiv:2503.10902*. https://arxiv.org/abs/2503.10902 (2025).
145. Phillips, P. J. et al. Experimental verification of orbital engineering at the atomic scale: Charge transfer and symmetry breaking in nickelate heterostructures. *Phys. Rev. B* **95**, 205131 (2017).
146. Lee, S. et al. Strong orbital polarization in a cobaltate-titanate oxide heterostructure. *Phys. Rev. Lett.* **123**, 117201 (2019).
147. Chandrasena, R. U. et al. Depth-resolved charge reconstruction at the $LaNiO_3$/$CaMnO_3$ interface. *Phys. Rev. B* **98**, 155103 (2018).
148. Paudel, J. R. et al. Direct experimental evidence of tunable charge transfer at the $LaNiO_3$/$CaMnO_3$ ferromagnetic interface. *Phys. Rev. B* **108**, 054441 (2023).
149. Mondal, D. et al. Modulation-doping a correlated electron insulator. *Nat. Commun.* **14**, 6210 (2023).
150. Paudel, J. R. et al. Depth-resolved profile of the interfacial ferromagnetism in $CaMnO_3$/$CaRuO_3$ superlattices. *Nano Lett.* **24**, 15195–15201 (2024).

151. Jiang, J. et al. Electronic properties of epitaxial $La_{1-x}Sr_xRhO_3$ thin films. *Phys. Rev. B* **103**, 195153 (2021).
152. Sohn, B. et al. Observation of orbital selective charge transfer in a $Fe/BaTiO_3$ interfacial two-dimensional electron gas. *Phys. Rev. B* **109**, 155106 (2024).
153. Cao, Y. et al. Tunable correlated states and spin-polarized phases in twisted bilayer–bilayer graphene. *Nature* **583**, 215–220 (2020).
154. Zhang, H. et al. Observation of dichotomic field-tunable electronic structure in twisted monolayer-bilayer graphene. *Nat. Commun.* **15**, 3737 (2024).
155. Zhou, Z. et al. Gate-tunable double-dome superconductivity in twisted trilayer graphene. *Nat. Phys.* **21**, 1773–1779 (2025).
156. Kotliar, G. & Liu, J. Superexchange mechanism and *d*-wave superconductivity. *Phys. Rev. B* **38**, 5142–5145 (1988).
157. White, S. R. Density-matrix algorithms for quantum renormalization groups. *Phys. Rev. B* **48**, 10345–10356 (1993).
158. Lee, Y. L., Lee, Y. W., Mou, C.-Y. & Weng, Z. Y. Two-leg *t–J* ladder: a mean-field description. *Phys. Rev. B* **60**, 13418–13428 (1999).
159. Jutho et al. Jutho/tensorkit.jl: v0.12.7. https://doi.org/10.5281/zenodo.13950435 (2024).
160. Li, Q. FiniteMPS.jl. https://github.com/Qiaoyi-Li/FiniteMPS.jl (2025).
161. Weichselbaum, A. Non-abelian symmetries in tensor networks: a quantum symmetry space approach. *Ann. Phys.* **327**, 2972–3047 (2012).
162. Weichselbaum, A. X-symbols for non-abelian symmetries in tensor networks. *Phys. Rev. Res.* **2**, 023385 (2020).

Acknowledgements

We are grateful to the stimulating discussions with Chen Lu. F. Y. and C. W. is supported by the National Natural Science Foundation of China (NSFC) under the Grant No. 12234016. F. Y. is also supported by the CAS Superconducting Research Project under Grant No. [SCZX-0101] and the NSFC under the Grant No. 12074031. C. W. is also supported by the NSFC under the Grant No. 12174317. D. X. Y. is supported by NSFC-12494591, NSFC-92165204, NSFC-92565303, NKRDPC-2022YFA1402802, Research Center for Magnetoelectric Physics of Guangdong Province (2024B0303390001), and Guangdong Provincial Quantum Science Strategic Initiative (GDZX2401010). C. W. is also supported by the New Cornerstone Science Foundation.

Author contributions

F. Yang proposed the main idea and supervised the study. Z.-Y. Shao performed the SBMF study. J.-H. Ji performed the DMRG study. D.-X. Yao and C. Wu helped shape the main idea. F. Yang, Z.-Y. Shao and J.-H. Ji wrote the paper. All authors contributed significantly to the data analysis and discussion.

Competing interests

The authors declare no competing interests.

Additional information

Supplementary information The online version contains supplementary material available at https://doi.org/10.1038/s41467-025-67880-5.

Correspondence and requests for materials should be addressed to Fan Yang.

Peer review information *Nature Communications* thanks the anonymous reviewers for their contribution to the peer review of this work. A peer review file is available.

Reprints and permissions information is available at http://www.nature.com/reprints

Publisher's note Springer Nature remains neutral with regard to jurisdictional claims in published maps and institutional affiliations.

Open Access This article is licensed under a Creative Commons Attribution-NonCommercial-NoDerivatives 4.0 International License, which permits any non-commercial use, sharing, distribution and reproduction in any medium or format, as long as you give appropriate credit to the original author(s) and the source, provide a link to the Creative Commons licence, and indicate if you modified the licensed material. You do not have permission under this licence to share adapted material derived from this article or parts of it. The images or other third party material in this article are included in the article's Creative Commons licence, unless indicated otherwise in a credit line to the material. If material is not included in the article's Creative Commons licence and your intended use is not permitted by statutory regulation or exceeds the permitted use, you will need to obtain permission directly from the copyright holder. To view a copy of this licence, visit http://creativecommons.org/licenses/by-nc-nd/4.0/.

© The Author(s) 2026